Selection of Radial Basis Functions for the Accuracy of Meshfree Galerkin Method in Rotating Euler–Bernoulli Beam Problem

Vijay Panchore[1]

Abstract

In this work, the radial basis function approximations are used to improve the accuracy of meshfree Galerkin method. The method is applied to the free vibration problems of non-rotating and rotating Euler–Bernoulli beams. The stiffness and mass matrices are derived by using conventional methods. In this meshfree method, only six nodes are considered within a single sub-domain. The parameters are varied for different approximations; the results are obtained with different approximations and found accurate. Two new basis function have been developed which are relatively accurate than conventional basis function: the first new basis function is obtained by multiplication of linear function to radial basis function and second new basis function is obtained by multiplying cubuic radial basis function to Gaussian radial basis function. The first few modes show same result that is available in literature using finite element method and higher modes are found very accurate as well. The result are found to be more accurate for first three modes of non-rotating and rotating Euler–Bernoulli beams where the cantilever beam boundary conditions are used; the first three modes do not change with the change in the parameter c of radial basis function.

Keywords Radial basis function · Mechanical vibration · Meshfree Galerkin method · Rotating Euler–Bernoulli beam

Introduction

Radial basis functions are frequently used in numerical methods; the meshfree method is used for structural problems where it is superior to conventional finite element method. Generally, moving least squares functions are used in formulation of meshfree method but it does not satisfy the Kronecker delta property like radial basis functions; it is easier to apply the essential boundary conditions with radial basis functions. The selection of parameters for radial basis functions plays an important role for the accuracy of method. Also, it depends

✉ Vijay Panchore
vijaypanchore36@gmail.com

1 Department of Mechanical Engineering, Maulana Azad National Institute of Technology, Bhopal 462003, India

121 Page 2 of 17

Int. J. Appl. Comput. Math (2022) 8:121

on the problem which we solve. Number of solutions can be obtained with changing the parameters of radial basis function: in meshfree methods the length of the subdomain may change and accurate results can be obtained with only few nodes. The meshfree Galerkin method can be used to conclude the results using radial basis function.

The traditional Galerkin method and Galerkin finite element method are generally used. The governing partial differential equation of rotating Euler–Bernoulli beam has been solved with traditional Galerkin method, Galerkin finite element method and Galerkin meshfree method. In Galerkin meshfree method, the subdomain for trial and test functions remains same; we have to be careful with selection of basis functions. The Petrov–Galerkin method which is a truly meshless method has explored in literature as well with radial basis functions. It is very essential to select the parameters of radial basis functions based on the problem. In literature, it is also found that summation of two radial basis functions increases the subdomain length: increase in number of nodes within the subdomain. The stiffness matrix of a rotating Euler–Bernoulli beam has been converted in symmetric form in recent literature.

The radial basis functions are generally used in neural networks and other computations; the radial basis functions are used to solve the differential equations [1]. The collective approach of radial basis functions and finite element method has been used to solve the electromagnetic problems [2]. The radial basis functions which are self-organizing are used for the development of neural network [3]. These entire radial basis functions are assumed in its original form while the improvements can be done based on the nature of the problem. In numerical problems, radial basis functions are assumed as basis functions and results obtained are accurate; the higher order derivatives of a radial basis function can be computed easily. The radial basis function has been frequently used with meshfree methods as well where the shape functions are defined on the nodes.

The meshless methods have relative advantage in few areas to finite element method: In problems of structures having cracks, the nodes can be placed at the location of crack and the analysis can be done. The meshfree methods have been used with different basis function: (1) moving least squares basis function, (2) basis functions derived from Kriging polynomial and (3) radial basis function. The advantage of radial basis function is that it does satisfy the Kronecker delta property and the essential boundary conditions can be applied easily. The formulation involves mostly Galerkin method or Petrov–Galerkin method. To check the initial results of the method Galerkin method can be used where the subdomain of trial and test function is same.

The basic accuracy has been discussed with the combination of meshless method and radial basis function [4]. The Dirichlet problems have been solved using this combination [5]. The Navier–Stokes equation has also been solved where results show good agreement with literature [6]. Partial differential equations have been solved with this combination [7]. The collocation method has been used to solve the partial differential equation with similar combination of meshless method and radial basis function [8]. The radial basis function interpolation along with the barycentric rational interpolation has been used to 2D viscoelastic wave equation [9]. The global and local meshless method has been used for solving problems of incompressible fluid flow with heat transfer where radial basis functions have been used [10]. Kernel Techniques have also been used for meshless methods [11].

The ordinary differential equations followed by high order L-stable method have been discussed in literature [12]. The partial differential equations have been solved using the integrated multi quadric radial basis function approximation methods [13]. The radial basis functions with finite difference method have been discussed in literature [14]. The unsteady Burgers' equation has been solved using the meshless methods where radial basis functions are used as basis functions [15]. On arbitrary surfaces, the partial differential equations are

solved by orthogonal gradients method where basis functions are radial basis functions [16]. A unique stable basis for the interpolation using radial basis function has been discussed as well [17]. The advection–diffusion-reaction equations have been solved using the local radial basis function method [18]. Non local boundary value problems with Neumann's boundary conditions are solved using the radial basis function method [19]. In literature, the orthogonal polynomials have also been used as basis functions in meshless method approximation.

An analytical solution has been obtained with the combination of orthogonal polynomials and Walsh function for fractional transport equation [20]. The general fractional model of COVID-19 has been comparatively studied with the effects of isolation and quarantine where general fractional model provides better results when compared to conventional methods [21]. A novel fractional chaotic system has been studied where quadratic and cubic nonlinearities are considered and a nonstandard finite difference scheme is used [22]. The motion of a beam on nanowire has been studied where Lagrangian and fractional Euler-Lagrangian equations [23]. A similar formulation has been used for capacitor microphone case study [24]. A fractional hybrid integro-differential equation with mixed hybrid integral boundary value conditioned was investigated which leads to less material consumption [25]. A new fractional hybrid value problem has been explored with examples [26]. The solution for fractional differential inclusions has been studied which is useful in solving real world problems [27]. The extensions of fractional thermostat model were provided using the solved examples [28].

The Caputo-Fabrizio fractional modeling has been used to study the hearing loss due to Mumps virus [29]. It has also been used to analyze transient response of the parallel RCL circuit [30]. The generalized Caputo fractional derivatives were used to investigate the p-Laplacian nonperiodic nonlinear boundary value problem [31]. In the recent literature, the extended fractional Caputo-Fabrizio derivation has been used for fractional integro-differential inclusions [32]. This derivative has also been applied to higher order fractional integro-differential equations and to analyze the model of HIV-1 infection of CD4 + T-cell [33, 34]. The new class of hybrid type fractional differential equations has been solved where the examples are provided as well [26].

In this paper, we solve the free vibration problem of rotating Euler–Bernoulli beam using the meshless method where radial basis functions are used. Generally, the problem is solved using the finite element method [35–38]. The non-rotating beam solutions are also obtained by using the meshless method where radial basis functions are used [39]. The parameter used in radial basis function approximation is never explored. In this study, we change the parameter of radial basis function to get accurate solutions of rotating beams. Also, based on the concept of centrifugal force which varies along the length of the beam, we develop a new basis function which is found to be more accurate for the first three modes. The results are discussed in detail where only one sub-domain is considered for trial and test functions. The accurate values of this problem have been obtained in recent literature [40]. The results include the non-rotating and rotating Euler–Bernoulli beam and non-uniform rotating and non-uniform non-rotating beam as well. The solutions can be obtained with numbers of techniques where the radial basis functions are used for weak form of Petrov–Galerkin method. Here we choose this method and notice the change in parameters which influence the results.

Formulation in Weak Form

The partial differential equation for a rotating Euler–Bernoulli beam is given by

$$\frac{\partial^2}{\partial x^2}\left(EI(x)\frac{\partial^2 w(x,t)}{\partial x^2}\right) + m(x)\frac{\partial^2 w(x,t)}{\partial t^2} - \frac{\partial}{\partial x}\left(G(x)\frac{\partial w(x,t)}{\partial x}\right) = 0 \qquad (1)$$

For a fixed free beam the boundary conditions and initial conditions are given by $w(0,t) = 0$, $\frac{\partial w(0,t)}{\partial x} = 0$, $EI\frac{\partial^2 w(R,t)}{\partial x^2} = 0$, $EI\frac{\partial^3 w(R,t)}{\partial x^3} - G(R)\frac{\partial w(R,t)}{\partial x} = 0$, $w(x,0) = w_0(x)$ and $\frac{\partial w(x,0)}{\partial x} = \dot{w}_0(x)$. where, $0 \leq x \leq R$ and $0 \leq t \leq 2\pi$.

Here, the flexural stiffness is $EI(x)$, mass per unit length is $m(x)$.

$G(x)$ is the centrifugal force which is given by

$$G(x) = \int_x^R m(x)\Omega^2 x dx \qquad (2)$$

where, Ω is the angular velocity and R is the radius of the rotating beam.

The centrifugal force for a rotating beam is maximum at the root while minimum at the free end. Figure 1 shows a rotating Euler–Bernoulli beam.

The problem will be an ordinary differential equation after substituting $w(x,t) = e^{i\omega t}\overline{w}(x)$ to get

$$\frac{d^2}{dx^2}\left(EI(x)\frac{d^2\overline{w}(x)}{dx^2}\right) - m(x)\omega^2\overline{w}(x) - \frac{d}{dx}\left(G(x)\frac{d\overline{w}(x)}{dx}\right) = 0 \qquad (3)$$

The flexural stiffness and mass per unit length will be constant for a uniform beam and the equation can be written as

$$EI\frac{d^4\overline{w}(x)}{dx^4} - m\omega^2\overline{w}(x) - \frac{d}{dx}\left(G(x)\frac{d\overline{w}(x)}{dx}\right) = 0 \qquad (4)$$

where, ω is the natural frequency.

The weak form of Eq. (4) is given by

$$\int_0^R v(x)\left\{EI\frac{d^4\overline{w}(x)}{dx^4} - m\omega^2\overline{w}(x) - \frac{d}{dx}\left(G(x)\frac{d\overline{w}(x)}{dx}\right)\right\}dx = 0 \qquad (5)$$
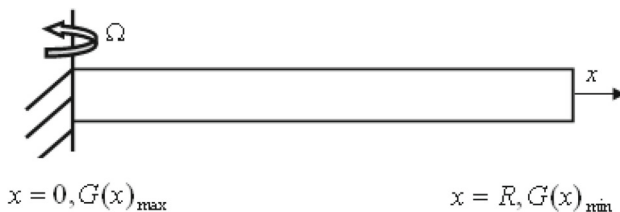
where, $v(x)$ is the test function.

Fig. 1 A rotating Euler–Bernoulli beam

Stiffness and Mass Matrices of Rotating Euler–Bernoulli Beam

Equation 5 is integrated by parts to get

$$\left[v(x)EI\frac{d^3\overline{w}(x)}{dx^3}\right]_0^R - \left[\frac{dv(x)}{dx}EI\frac{d^2\overline{w}(x)}{dx^2}\right]_0^R + \int_0^R EI\frac{d^2v(x)}{dx^2}\frac{d^2\overline{w}(x)}{dx^2}dx - \left[v(x)G(x)\frac{d\overline{w}(x)}{dx}\right]_0^R$$

$$+ \int_0^R G(x)\frac{dv(x)}{dx}\frac{d\overline{w}(x)}{dx}dx - m\omega^2\int_0^R v(x)\overline{w}(x)dx = 0 \tag{6}$$

$$\left[v(x)\left\{EI\frac{d^3\overline{w}(x)}{dx^3} - G(x)\frac{d\overline{w}(x)}{dx}\right\}\right]_0^R - \left[EI\frac{dv(x)}{dx}\frac{d^2\overline{w}(x)}{dx^2}\right]_0^R + \int_0^R EI\frac{d^2v(x)}{dx^2}\frac{d^2\overline{w}(x)}{dx^2}dx$$

$$+ \int_0^R G(x)\frac{dv(x)}{dx}\frac{d\overline{w}(x)}{dx}dx - m\omega^2\int_0^R v(x)\overline{w}(x)dx = 0 \tag{7}$$

Writing $\overline{w}(x) = [N(x)][q]$ and $v(x) = [q]^T[N(x)]^T$, we get

$$\left[EI[N]^T\frac{d^3[N]^T}{dx} - G(x)[N]^T\frac{d[N]}{dx}\right]_0^R [q] - \left[EI\frac{d[N]^T}{dx}\frac{d^2[N]}{dx^2}\right][q]$$

$$+ \left\{\int_0^R EI\frac{d^2[N]^T}{dx^2}\frac{d^2[N]}{dx^2}dx + \int_0^R G(x)\frac{d[N]^T}{dx}\frac{d[N]}{dx}dx\right\}[q] - \left\{m\omega^2\int_0^R [N]^T[N]dx\right\}[q] = 0 \tag{8}$$

The terms outside the integral will be zero as we satisfy the natural boundary conditions. Then we get

$$\left\{\int_0^R EI\frac{d^2[N]^T}{dx^2}\frac{d^2[N]}{dx^2}dx + \int_0^R G(x)\frac{d[N]^T}{dx}\frac{d[N]}{dx}dx\right\}[q] - \left\{m\omega^2\int_0^R [N]^T[N]dx\right\}[q] = 0 \tag{9}$$

The mass and stiffness matrices are given by

$$[K] = \int_0^R EI\frac{d^2[N]^T}{dx^2}\frac{d^2[N]}{dx^2}dx + \int_0^R G(x)\frac{d[N]^T}{dx}\frac{d[N]}{dx}dx \tag{10}$$

$$[M] = m\int_0^R [N]^T[N]dx \tag{11}$$

Radial Basis Function Interpolation for Meshfree Method

The test and trial functions are similar in Galerkin method and are having the same sub-domain length ($\Omega_s^{(1)}$).
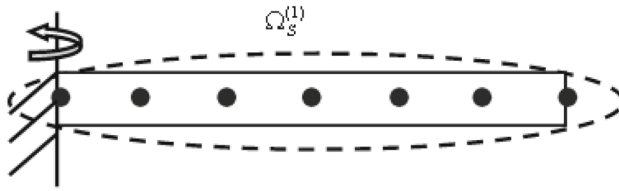
Fig. 2 Distributions of nodes

Figure 2 shows the distribution of the nodes in a rotating Euler–Bernoulli beam. In the current study only six nodes are considered for the subdomain of trial and test function.

The transverse displacement of an Euler–Bernoulli beam is given by

$$\overline{w}(x) = R_1(x)a_1 + S_1(x)b_1 + R_2(x)a_2 + S_2(x)b_2 + \ldots + R_N(x)a_N + S_N(x)b_N \quad (12)$$

where, $a_1, b_1, a_2, b_2, \ldots, a_N, b_N$ are arbitrary constants. The radial basis function is given by

$$R_j(x) = e^{-c\frac{(|x-x_j|)^2}{s_j^2}} \quad (13)$$

Generally, the value of c is considered as one. In the present study we explore the values for $c = 1, \frac{1}{2}, \frac{1}{5}, \frac{1}{10}, \frac{1}{50}, \frac{1}{100}$

The derivative of radial basis function is given by

$$S_j(x) = \frac{dR_j(x)}{dx} \quad (14)$$

Values of c and s_j are user defined. The slope is given by

$$\theta(x) = \frac{dR_1(x)}{dx}a_1 + \frac{dS_1(x)}{dx}b_1 + \frac{dR_2(x)}{dx}a_2 + \frac{dS_2(x)}{dx}b_2 + \ldots + \frac{dR_N(x)}{dx}a_N + \frac{dS_N(x)}{dx}b_N \quad (15)$$

We can then rewrite the transverse displacement as

$$\overline{w}(x) = [Q(x)]_{(1,2N)}[c]^T_{(2N,1)} \quad (16)$$

where,

$$[Q(x)]_{(1,2N)} = [R_1(x)S_1(x)R_2(x)S_2(x)\ldots R_N(x)S_N(x)] \quad (17)$$

and

$$[c]_{(1,2N)} = [a_1b_1a_2b_2\ldots a_Nb_N] \quad (18)$$

The slope can be given as

$$\theta(x) = \left[\frac{dQ(x)}{dx}\right]_{(1,2N)}[c]^T_{(2N,1)} \quad (19)$$

where,

$$\left[\frac{dQ(x)}{dx}\right]_{(1,2N)} = \left[\frac{dR_1(x)}{dx}\frac{dS_1(x)}{dx}\frac{dR_2(x)}{dx}\frac{dS_2(x)}{dx}\ldots\frac{dR_N(x)}{dx}\frac{dS_N(x)}{dx}\right] \quad (20)$$

Eventually the assembled equation can be written as

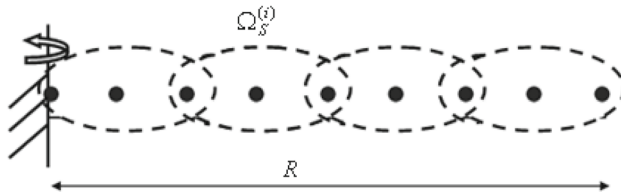$$[Q_M]_{(2N,2N)}[c]^T_{(2N,1)} = [d]_{(2N,1)} \quad (21)$$

Fig. 3 Multiple subdomain with in a rotating Euler–Bernoulli beam

where,

$$[d]_{(1,2N)} = [w_1 \theta_1 w_2 \theta_2 \ldots w_N \theta_N] \tag{22}$$

and

$$[Q_M] = \begin{bmatrix} R_1(x_1) & S_1(x_1) & R_2(x_1) & S_2(x_1) & \ldots & R_N(x_1) & S_N(x_1) \\ \frac{dR_1(x_1)}{dx} & \frac{dS_1(x_1)}{dx} & \frac{dR_2(x_1)}{dx} & \frac{dS_2(x_1)}{dx} & \ldots & \frac{dR_N(x_1)}{dx} & \frac{dS_N(x_1)}{dx} \\ R_1(x_2) & S_1(x_2) & R_2(x_2) & S_2(x_2) & \ldots & R_N(x_2) & S_N(x_2) \\ \frac{dR_1(x_2)}{dx} & \frac{dS_1(x_2)}{dx} & \frac{dR_2(x_2)}{dx} & \frac{dS_2(x_2)}{dx} & \ldots & \frac{dR_N(x_2)}{dx} & \frac{dS_N(x_2)}{dx} \\ \vdots & \vdots & \vdots & \vdots & \vdots & \vdots & \vdots \\ R_1(x_N) & S_1(x_N) & R_2(x_N) & S_2(x_N) & \ldots & R_N(x_N) & S_N(x_N) \\ \frac{dR_1(x_N)}{dx} & \frac{dS_1(x_N)}{dx} & \frac{dR_2(x_N)}{dx} & \frac{dS_2(x_N)}{dx} & \ldots & \frac{dR_N(x_N)}{dx} & \frac{dS_N(x_N)}{dx} \end{bmatrix} \tag{23}$$

Here, $w_1, \theta_1, w_2, \theta_2, \ldots, w_N, \theta_N$ are the nodal degrees of freedom.
Rewriting Eq. 21, we get

$$[c]^T_{(2N,1)} = [Q_M]^{-1}_{(2N,2N)}[d]_{(2N,1)} \tag{24}$$

The transverse displacement can be given as

$$\overline{w}(x) = [H(x)]_{(1,2N)}[d]_{(2N,1)} \tag{25}$$

where, $[H(x)]$ is the shape function vector.

$$\begin{aligned} [H(x)]_{(1,2N)} &= [Q(x)]_{(1,2N)} [Q_M]^{-1}_{(2N,2N)} \\ &= \left[\phi_1^{(w)}(x) \phi_1^{(\theta)}(x) \phi_2^{(w)}(x) \phi_2^{(\theta)}(x) \ldots \phi_N^{(w)}(x) \phi_N^{(\theta)}(x) \right] \end{aligned} \tag{26}$$

Here, $\phi_i^{(w)}(x)$ and $\phi_i^{(\theta)}(x)$ are the shape functions associated with node i.
We can then write transverse displacement as

$$\overline{w}(x) = \sum_{j=1}^{N} \left(\phi_j^{(w)}(x)w_j + \phi_j^{(\theta)}(x)\theta_j \right) \tag{27}$$

In meshfree Galerkin method, we assume the test function similar to the trial function and it is given by

$$v(x) = \sum_{j=1}^{N} \left(\phi_j^{(w)}(x)\delta w_j + \phi_j^{(\theta)}(x)\delta \theta_j \right) \tag{28}$$

121   Page 8 of 17

Int. J. Appl. Comput. Math (2022) 8:121

Table 1 Natural frequencies for rotating speed $s = 0$.

Mode	Baseline [40]	For $c = 1$	For $c = 1/2$	For $c = 1/5$	For $c = 1/10$	For $c = 1/20$	For $c = 1/50$	For $c = 1/100$
η_1	3.5160	3.4327	3.5153	3.5160	3.5160	3.5160	3.5160	3.5160
η_2	22.0345	21.8211	22.0317	22.0345	22.0345	22.0345	22.0345	22.0345
η_3	61.6972	59.9602	61.6462	61.6969	61.6972	61.6972	61.6972	61.6972
η_4	120.902	107.3111	120.2881	120.9004	120.9014	120.9035	120.9050	120.9056
η_5	199.860	161.1016	196.6828	199.6985	199.7866	199.6969	199.6111	199.5789

Table 2 Natural frequencies for rotating speed $s = 12$.

Mode	Baseline [40]	For $c = 1$	For $c = 1/2$	For $c = 1/5$	For $c = 1/10$	For $c = 1/20$	For $c = 1/50$	For $c = 1/100$
η_1	13.1702	13.5361	13.1739	13.1702	13.1702	13.1702	13.1702	13.1702
η_2	37.6031	38.0095	37.6085	37.6031	37.6031	37.6031	37.6031	37.6031
η_3	79.6145	80.4304	79.6593	79.6154	79.6145	79.6145	79.6145	79.6145
η_4	140.534	139.4396	140.3138	140.5324	140.5380	140.5382	140.5372	140.5367
η_5	220.536	208.8860	218.8318	220.1734	220.2223	220.1908	220.1655	220.1578

121 Page 10 of 17

Int. J. Appl. Comput. Math (2022) 8:121

Table 3 Natural frequencies for rotating speed $s = 0$.

Mode	Baseline [40]	For $c = 1$	For $c = 1/2$	For $c = 1/5$	For $c = 1/10$	For $c = 1/20$	For $c = 1/50$	For $c = 1/100$
η_1	3.5160	3.4801	3.5156	3.5160	3.5160	3.5160	3.5160	3.5160
η_2	22.0345	22.1875	22.0370	22.0345	22.0345	22.0345	22.0345	22.0345
η_3	61.6972	59.5934	61.6577	61.6969	61.6972	61.6972	61.6972	61.6972
η_4	120.902	95.5824	120.1302	120.8993	120.9014	120.9035	120.9050	120.9054
η_5	199.860	174.6122	197.1752	199.7082	199.7857	199.6964	199.6110	199.5789

Table 4 Natural frequencies for rotating speed $s = 12$.

| Mode	Baseline [40]	For $c = 1$	For $c = 1/2$	For $c = 1/5$	For $c = 1/10$	For $c = 1/20$	For $c = 1/50$	For $c = 1/100$
η_1	13.1702	13.3645	13.1729	13.1702	13.1702	13.1702	13.1702	13.1702
η_2	37.6031	37.8680	37.6083	37.6031	37.6031	37.6031	37.6031	37.6031
η_3	79.6145	80.5298	79.6621	79.6153	79.6146	79.6145	79.6145	79.6145
η_4	140.534	137.2617	140.2341	140.5321	140.5380	140.5382	140.5372	140.5367
η_5	220.536	211.5172	219.0702	22.1800	220.2212	220.1902	220.1654	220.1577
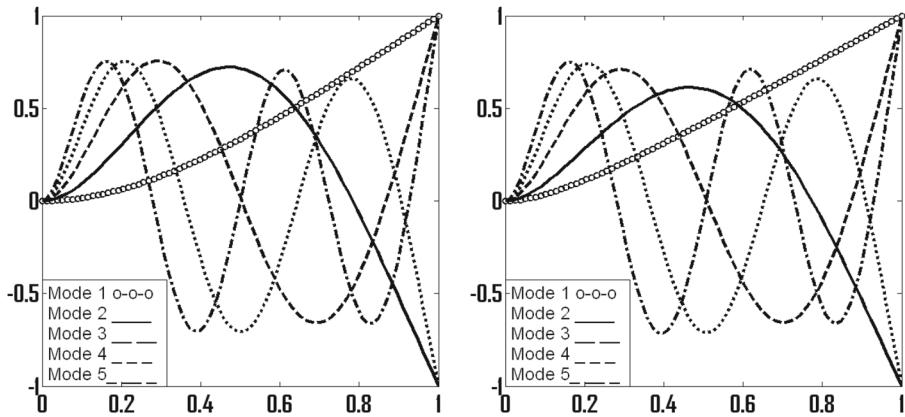
Fig. 4 1 and 2 Mode shapes of a uniform beam for rotating speed $s = 0$ (left) and $s = 12$ (right) for $P(x)$

The mass matrix and stiffness matrix for each subdomain is given by

$$[K]_{\Omega_S^{(i)}} = EI \int\limits_{\Omega_S^{(i)}} \left[H''(x)\right]^{\mathrm{T}}\left[H''(x)\right]dx + \frac{m\Omega^2}{2} \int\limits_{\Omega_s^{(i)}} (R^2 - x^2)\left[H'(x)\right]^{\mathrm{T}}\left[H'(x)\right]dx \quad (29)$$

$$[M]_{\Omega_S^{(i)}} = m \int\limits_{\Omega_S^{(i)}} [H(x)]^{\mathrm{T}}[H(x)]dx \quad (30)$$

In case of multiple subdomain the assembly is required. Figure 3 shows the multiple subdomains.

Formulation of a New Basis Function

In case of rotating Euler–Bernoulli beam, the centrifugal force varies along the length. To capture this, the radial basis function is multiplied with function x. The resulting function is given by

$$P_j(x) = xR_j(x) = xe^{-c\frac{(|x-x_j|)^2}{s_j^2}} \quad (31)$$

The results show that the first, second, and third mode can be relatively accurate when we use above basis functions. The rest of the procedure is similar to radial basis function approximation.

The Gaussian radial basis function when multiplied to cubic radial basis function the approximation is give by

$$Q_j(x) = \left(|x-x_j|\right)^3 e^{-c\frac{(|x-x_j|)^2}{s_j^2}} \quad (32)$$

Table 5 Natural frequencies for rotating speed $s = 0$.

Mode	Baseline [40]	For $c = 1$	For $c = 1/2$	For $c = 1/5$	For $c = 1/10$	For $c = 1/20$	For $c = 1/50$	For $c = 1/100$
η_1	3.5160	1.7068	3.5107	3.5160	3.5160	3.5160	3.5160	3.5160
η_2	22.0345	18.0205	21.9610	22.0345	22.0345	22.0345	22.0345	22.0345
η_3	61.6972	43.1810	61.4146	61.6968	61.6972	61.6972	61.6972	61.6972
η_4	120.902	96.0747	116.2223	120.8900	120.9011	120.9034	120.9054	120.9058
η_5	199.860	179.7362	193.6771	199.6727	199.7921	199.6719	199.5674	199.5385

Table 6 Natural frequencies for rotating speed $s = 12$.

| Mode	Baseline [40]	For $c = 1$	For $c = 1/2$	For $c = 1/5$	For $c = 1/10$	For $c = 1/20$	For $c = 1/50$	For $c = 1/100$
η_1	13.1702	40.4605	13.4832	13.1702	13.1702	13.1702	13.1702	13.1702
η_2	37.6031	53.9286	37.6245	37.6031	37.6031	37.6031	37.6031	37.6031
η_3	79.6145	112.0052	80.5385	79.6162	79.6145	79.6145	79.6145	79.6145
η_4	140.534	185.0880	140.5990	140.5315	140.5384	140.5384	140.5367	140.5360
η_5	220.536	314.0903	218.8445	220.1212	220.2186	220.1813	220.1544	220.1491
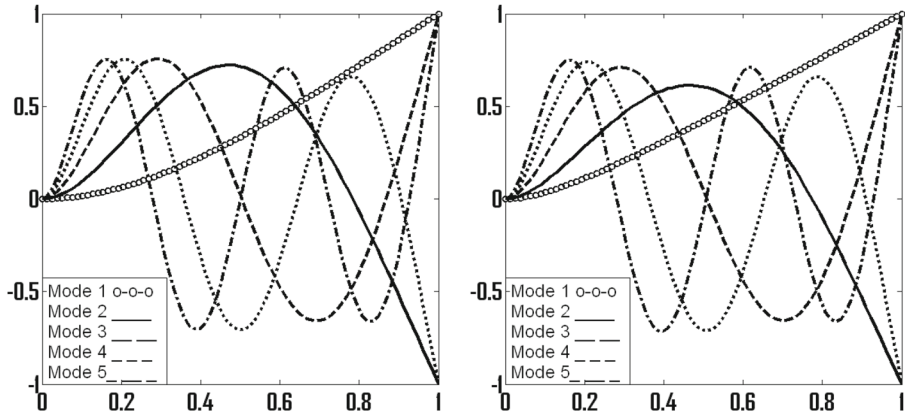
Fig. 5 1 and 2 Mode shapes of a uniform beam for rotating speed $s = 0$ (left) and $s = 12$ (right) for $Q(x)$

Results

Results are obtained for a single sub-domain where six nodes are considered in each sub-domain. The results are obtained for the value of $c = 1, \frac{1}{2}, \frac{1}{5}, \frac{1}{10}, \frac{1}{50}, \frac{1}{100}$ Both non-rotating and rotating beams are considered here. Tables 1 and 2 show the results for non-rotating and rotating beam respectively. Non-dimensional rotating frequency η and non-dimensional rotating speed s is given by $\eta = \omega \sqrt{\frac{m_0 R^4}{E I_0}}$, $s = \Omega \sqrt{\frac{m_0 R^4}{E I_0}}$.

The results show that value of c should not be one and the tables show the accuracy when the values are less than one. The exact values can be obtained using trial and error where the values are similar to the conventional finite element method. The results of new basis function $P_j(x)$ are given in Tables 3 and 4. Figure 4 shows the respective mode shapes.

The results of new basis function $Q_j(x)$ are given in Tables 5 and 6. Figure 5 show the respective mode shapes. Here in Table 5, the results are not accurate for $c = 1$ and $c = 0.5$ which clearly show the importance of approximation. The similar observation can be seen in Table 6.

Conclusions

The parameter (c) has been varied to get the approximate solutions; we observed that for better accuracy the values of c are in between 1 and 0.01. The results get accuracy for the decreasing value of c. The results are obtained for non-rotating and rotating Euler–Bernoulli beams. The two new basis functions which have been developed provide better results for the first three modes when compared to conventional method. The stiffness and mass matrices have been derived for meshfree method. The results are found for a fixed-free beam, which are accurate while considering only six nodes within the sub-domain of trial and test function. The new basis function is introduced to see the effect of centrifugal force in the solution. The results clearly show the importance of approximation in numerical methods: finite element method and meshfree methods. These methods can be applied to a numbers of problems such as Rayleigh beam theory and Timoshenko beam theory where the results may or may not vary with change in radial basis function paramter c. The results will also vary with numebrs

on nodes within the sub-domain of trial function. One more important observation is for second new basis function the results are not accurate for $c = 1$ and $c = 0.5$. The radial basis function is having numbers of approximations: Gaussian functions, multi-quadric functions and thin plate spline functon. These approximations provides results which are not similar as we change the parameters.

Data Availability   The mathematical codes will not be available while other datas can be shared by author.

Declarations

Conflict of interest   On behalf of all authors, the corresponding author states that there is no conflict of interest.

References

1. Kumar, M., Yadav, N.: Multilayer perceptrons and radial basis function neural network methods for the solution of differential equations: a survey. Comput. Math. Appl. **62**, 3796–3811 (2011)
2. Zou, Y., Lie, G., Shao, K., Guo, Y., Zhu, J., Chen, X.: Hybrid approach of radial basis function and finite element method for electromagnetic problems. IEEE Trans. Mag. **51**, 1–4 (2015)
3. Han, H., Chen, Q., Qiao, J.: Research on an online self-organizing radial basis function neural network. Neural Comput. Appl. **19**, 667–676 (2010)
4. Duan, Y.: A note on the meshless method using radial basis functions. Comput. Math. Appl. **55**, 66–75 (2008)
5. Duan, Y., Tan, Y.-J.: A meshless Galerkin method for Dirichlet problems using radial basis functions. J. Comput. Appl. Math. **196**, 394–401 (2006)
6. Chinchapatnam, P.P., Djidjeli, K., Nair, P.B.: Radial basis function meshless method for the steady incompressible Navier-Stokes equations. Int. J. Comput. Math. **84**, 1509–1526 (2007)
7. Wendland, H.: Meshless Galerkin methods using radial basis functions. Math. Comput. **68**, 1521–2153 (1999)
8. Zhang, X., Song, K.Z., Lu, M.W., Liu, X.: Mehsless methods based on collocation with radial basis functions. Comput. Mech. **26**, 333–343 (2000)
9. Oruc, O.: Two meshless methods based on local radial basis function and barycentric rational interpolation for solving 2D viscoelastic wave equation. Comput. Math. Appl. **79**, 3272–3288 (2020)
10. Waters, J., Pepper, D.W.: Global versus localized RBF meshless methods for solving incompressible fluid flow with heat transfer. Numer. Heat Transf. B. **68**, 185–203 (2015)
11. Schaback, R., Wendland, H.: Kernel techniques: from machine learning to meshless methods. Acta Numer. **15**, 1–97 (2006)
12. Kadalbajoo, M.K., Kumar, A., Tripathi, L.P.: Application of radial basis function with L-stable Padé time marching scheme for pricing exotic option. Comput. Math. Appl. **66**, 500–511 (2013)
13. Sarra, S.A.: Integrated multiquadric radial basis function approximation methods. Comput. Math. Appl. **51**, 500–511 (2006)
14. Fornberg, B., Lehto, E., Powell, C.: Stable calculation of Gaussian-based RBF-FD stencils. Comput. Math. Appl. **65**, 627–637 (2013)
15. Bouhamidi, A., Hached, M., Jbilou, K.: A meshless RBF method for computing a numerical solution of unsteady Burgers'-type equations. Comput. Math. Appl. **68**, 238–256 (2014)
16. Piret, C.: The orthogonal gradients method: a radial basis functions method for solving partial differential equations on arbitrary surfaces. J. Comput. Phys. **231**, 4662–4675 (2012)
17. Marchi, S.D., Santin, G.: A new stable basis for radial basis function interpolation. J. Comput. Appl. Math. **253**, 1–13 (2013)
18. Sarra, S.A.: A local radial basis function method for advection-diffusion-reaction equations on complexly shaped domains. Appl. Math. Comput. **218**, 9853–9865 (2012)
19. Kazem, S., Rad, J.A.: Radial basis functions method for solving of a non-local boundary value problem with Neumann's boundary conditions. Appl. Math. Model. **36**, 2360–2369 (2012)
20. Kadem, A., Baleanu, D.: Analytical method based on Walsh function combined with orthogonal polynomial for fractional transport equation. Commun. Nonlinear Sci. Numer. Simul. **15**, 491–501 (2010)

21. Baleanu, D., Abadi, M.H., Jajarmi, A., Vahid, K.Z., Nieto, J.J.: A new comparative study on the general fractional model of COVID-19 with isolation and quarantine effects. Alexand. Eng. J. **61**, 4779–4791 (2022)

22. Baleanu, D., Zibaei, S., Namjoo, M., Jajarmi, A.: A nonstandard finite difference scheme for the modelling and nonidentical synchronization of a novel fractional chaotic system. Adv. Differ. Equ. (2021). https://doi.org/10.1186/s13662-021-03454-1

23. Erturk, V.S., Godwe, E., Baleanu, D., Kumar, P., Asad, J., Jajarmi, A.: Novel fractional-order Lagrangian to describe motion of beam on nanowire. Acta Phys. Polonica A. **140**, 265–272 (2021)

24. Jajarmi, A., Baleanu, D., Vahid, K.Z., Pirouz, H.M., Asad, J.H.: A new and general fractional Lagrangian approach: a capacitor microphone case study. Results Phys. (2021). https://doi.org/10.1016/j.rinp.2021.104950

25. Baleanu, D., Etemad, S., Rezapour, S.: On a fractional hybrid integro-differential equation with mixed hybrid integral boundary value conditions by using three operators. Alexand. Eng. J. **59**, 3019–3027 (2020)

26. Baleanu, D., Etemad, S., Pourrazi, S., Rezapour, S.: On the new fractional hybrid boundary value problems with three-point integral hybrid conditions. Adv. Differ. Equ. (2019). https://doi.org/10.1186/s13662-019-2407-7

27. Baleanu, D., Hedayati, V., Rezapour, S., Qurashi, M. M. A.: On two fraction differential inclusions. Springer, New York (2016). https://doi.org/10.1186/s40064-016-2564-z

28. Baleanu, D., Etemad, S., Rezapour, S.: A hybrid Caputo fractional modelling for thermostat with hybrid boundary value conditions. Bound. Value Prob. (2020). https://doi.org/10.1186/s13661-020-01361-0

29. Mohammadi, H., Kumar, S., Rezapour, S., Etemad, S.: A theoretical study of the Caputo-Fabrizio fractional modelling for hearing loss due to Mumps virus with optimal control. Chaos Solitons Fractals. (2021). https://doi.org/10.1016/j.chaos.2021.110668

30. Alizadeh, S., Baleanu, D., Rezapour, S.: Analyzing transient response of the parallel RCL circuit by using the Caputo-Fabrizio fractional derivative. Adv. Differ. Equ. (2020). https://doi.org/10.1186/s13662-020-2527-0

31. Matar, M.M., Abbas, M.I., Alzabut, J., Kabar, M.K.A., Etemad, S., Rezapour, S.: Investigation of the p-Laplacian nonperiodic nonlinear boundary value problem via generalized Caputo fractional derivatives. Adv. Differ. Equ. (2021). https://doi.org/10.1186/s13662-021-03228-9

32. Baleanu, D., Rezapour, S., Saberpour, Z.: On fractional integro-differential inclusions via the extended fractional Caputo-Fabrizio derivation. Bound. Value Probl. (2019). https://doi.org/10.1186/s13661-019-1194-0

33. Aydogan, M.S., Baleanu, D., Mousalou, A., Rezapour, S.: On higher order integro-differential equations including the Caputo-Fabrizio derivative. Bound. Value Probl. (2018). https://doi.org/10.1186/s13661-018-1008-9

34. Baleanu, D., Mohammadi, H., Rezapour, S.: Analysis of the model of HIV-1 infection of CD4+ T-Cell with a new approach of fractional derivative. Adv. Differ. Equ. (2020). https://doi.org/10.1186/s13662-020-02544-w

35. Hodges, H.D., Rutkowski, M.J.: Free-vibration analysis of rotating beams by a variable-order finite element method. AIAA J. **19**, 1459–1466 (1981)

36. Nagaraj, V.T., Shanthakumar, P.: Rotor blade vibration by the Galerkin finite element method. J. Sound Vib. **43**, 575–577 (1975)

37. Bauchau, O.A., Hong, C.H.: Finite element approach to rotor blade modeling. J. Am. Helicop. Soc. **32**, 60–67 (1987)

38. Hoa, S.V.: Vibration of a rotating beam with tip mass. J. Sound Vib. **67**, 369–381 (1979)

39. Raju, I. S., Phillips, D. R., Krishnamurthy, T.: A radial basis function approach in the meshless local Petrov–Galerkin method for Euler–Bernoulli beam problems. Comput. Mech.**34,** 464–474 (2204)

40. Wang, G., Wereley, N.M.: Free vibration analysis of rotating blades with uniform tapers. AIAA J. **42**, 2429–2437 (2004)